ACS Applied Materials and Interfaces. 10 (47): 40549-40559 (2018).

In situ Formation of $Er_{0.4}Bi_{1.6}O_3$ Protective Layer at Cobaltite Cathode/Y_2O_3-ZrO_2 Electrolyte Interface Under Solid Oxide Fuel Cells Operation Conditions

Shuai He,[a,1] Qi Zhang,[a,b,1] Giulio Maurizio,[a,c] Lorenzo Catellani,[a,c] Kongfa Chen,[b] Qibing Chang,[d] Massimo Santarelli,[c] and San Ping Jiang[*,a]

[a] Fuels and Energy Technology Institute & Western Australian School of Mines: Minerals, Energy and Chemical Engineering, Curtin University, Perth, WA 6102, Australia

[b] College of Materials Science and Engineering, Fuzhou University, Fuzhou, Fujian 350108, China

[c] Energy Department, Politecnico di Torino, Corso Duca degli Abruzzi 24, 10129 Torino, Italy.

[d] College of Materials Science and Engineering, Jingdezhen Ceramic Institute, Jingdezhen, Jiangxi 333403, China

[1] These authors contributed equally.
* Corresponding Author: s.jiang@curtin.edu.au (SP Jiang)

Keywords: solid oxide fuel cells; direct assembly; decoration; ESB-LSCFNb composite cathode; electrode/electrolyte interface; in situ formation of ESB interlayer.

Abstract:

Bismuth based oxides exhibit outstanding oxygen ionic conductivity and fast oxygen surface kinetics and have shown great potential as a highly active component for electrode materials in solid oxide fuel cells (SOFC). Herein, a Nb-doped $La_{0.6}Sr_{0.4}Co_{0.2}Fe_{0.7}Nb_{0.1}O_{3-\delta}$ (LSCFNb) electrode with 40% $Er_{0.4}Bi_{1.6}O_3$ (ESB) composite electrode was successfully fabricated by decoration method and directly assembled on barrier-layer-free yttrium stabilized zirconia (YSZ) electrolyte cells, achieving a peak power density of 1.32 W cm^{-2} and excellent stability

at 750^{o}C and 250 mAcm^{-2} for 100 hrs. ESB decoration also significantly reduces the activation energy from 214 kJ mol^{-1} for the O_2 reduction on pristine LSCFNb electrode to 98 kJ mol^{-1}. Further microstructural analysis reveals that there is a redistribution and migration of the ESB phase in the ESB-LSCFNb composite towards the YSZ electrolyte under the influence of cathodic polarization, forming a thin ESB layer at the cathode/YSZ electrolyte interface. The *in situ* formed ESB layer not only prevents the direct contact and subsequent reaction between segregated SrO and YSZ electrolyte, but also remarkably promotes the oxygen migration/diffusion at the interface for O_2 reduction reaction, resulting in a remarkable increase in power output and decrease in activation energy. The present study clearly demonstrated the in situ formation of a highly functional and active ESB protective layer at LSCFNb cobaltite cathode and YSZ electrolyte interface via ESB decorated LSCFNb composite cathode under SOFC operation conditions.

1. Introduction

Solid oxide fuel cells (SOFCs) are the most efficient energy conversion devices to electrochemically convert the chemical energy of fuels such as hydrogen and natural gas to electricity with intrinsically high efficiency, low pollutant emissions and flexible fuel options.[1-4] However, the development of conventional SOFCs operated at high temperatures of ~1000^{o}C has been retarded by problems of high manufacturing and maintenance cost and high performance degradation due to microstructure degradation,[5-7] cation inter-diffusion,[8-9] contamination[10-11] and chemical reactions at the electrode/electrolyte interface.[12-14] Thus, significant effort has been made to reduce the operating temperature to intermediate and low temperatures of 500-800^{o}C to increase the durability, thermal compatibility and thermal cycle capability and to reduce the fabrication and materials costs of SOFCs.[1, 15-16] With the reduction

in operating temperature, the cell performance is increasingly dominated by the polarization losses of electrode reactions, especially at the cathode side due to the slow oxygen reduction reaction (ORR).[17] Mixed ionic and electronic conducting (MIEC) material such as $La_{0.6}Sr_{0.4}Co_{0.2}Fe_{0.8}O_{3-\delta}$ (LSCF) is probably the most popular and studied cathode for intermediate and low temperature SOFCs because of its superior mixed electronic conductivity (~250 S cm^{-1} at 800ºC) [18] and oxygen ionic conductivity (~0.2 S cm^{-1} at 900ºC),[19-20] excellent oxygen surface exchange rate and high electrocatalytic activity for ORR.[21-26] Unfortunately, the activation energy of LSCF based cathode for ORR is in the range of 130-160 kJ mol^{-1}.[26-28] The high activation energy implies the significant increase of polarization resistance with the decrease of operating temperature for the reaction on LSCF based cathodes. Nevertheless, recent studies have shown the promising development of high performance cathode materials that are capable of operating at very low temperatures.[29-30] For example, Li et al.[31] synthesized a niobium and tantalum co-substituted $SrCo_{0.8}NbTa_{0.1}O_{3-\delta}$ perovskite cathode material, achieving a high peak power density of 1.2 W cm^{-2} at 500 ºC in a $Gd_{0.1}Ce_{0.9}O_{1.95}$ (GDC)-based anode supported cell. Zhu et al.[32] developed a $Sr_{0.95}Ag_{0.05}Nb_{0.1}Co_{0.9}O_{3-\delta}$ (SANC) high performance cathode material, which is able to exsolve A-site silver nanoparticles. The anode supported cell with the Ag decorated SANC cathode demonstrated a high power density of 1.11 W cm^{-2} at 500 ºC and stability for 140 h at a current density of 0.625 A cm^{-2}. In addition, Duan et al.[33] designed a Zr and Y co-doped $BaCo_{0.4}Fe_{0.4}Zr_{0.1}Y_{0.1}O_{3-\delta}$ (BCFZY0.1) perovskite cathode material, which exhibits a high ORR activity, excellent low temperature performance and long term operation stability. For instance, an anode-supported GDC electrolyte cell with the BCFZY0.1 cathode achieved a high power density of 0.97 W cm^{-2} at 500 ºC and is very stable for 2500 h.

Doped bismuth oxides such as erbium stabilized bismuth oxide (ESB) have been reported to possess excellent oxygen surface exchange kinetics and one to two orders of magnitude

larger ionic conductivities as compared to conventional yttria stabilized zirconia (YSZ) at intermediate and low temperatures (0.023 S cm^{-1} at 500 ^oC and 0.37 S cm^{-1} at 700 ^oC).[34-36] Doped bismuth oxides have been applied as electrolyte,[37] an interfacial layer between the electrolyte and cathode,[38-39] as well as an active component for $La_{0.8}Sr_{0.2}MnO_{3-\delta}$ (LSM),[40-41] $Pr_{0.5}Ba_{0.5}MnO_3$ [42] and composite cathodes.[43-45] However, due to its low melting point temperature, high reactivity and phase instability in reducing atmosphere, the adoption of doped bismuth oxide is not as popular as other oxygen ion conductors. There is also a concern in the incorporation of bismuth oxide into cobaltite perovskite electrodes due to its high reactivity with cobaltite materials.[46-48] For instance, Lee *et al*. investigated the compatibility between ESB and LSCF after been heated at 850 ^oC for 1 h and observed significant new phase formation.[46] ESB reacted with LSCF, forming a $La(Sr,Bi)CoO_{3-\delta}$ phase at the LSCF/ESB interface.[47] It was reported that LSCF started to react with yttria stabilized bismuth oxide (YSB) at 650^oC, but by infiltrating YSB into LSCF scaffold followed by 600^oC sintering, the performance of the YSB-LSCF cell with proton conducting electrolyte was significantly enhanced, reaching a peak power density of 167 mW cm^{-2} at 550 ^oC.[48]

Most recently, we have shown that the incorporation of ESB with LSM and $Sm_{0.95}Co_{0.95}Pd_{0.05}O_{3-\delta}$ (SmCPd) composite electrodes via a decoration technique without pre-sintering process at high temperatures significantly enhances the performance of the cathode.[49-50] For example, an anode supported YSZ electrolyte cell with directly assembled ESB decorated LSM cathode exhibited a peak power density of 1.62 W cm^{-2} at 750 ^oC, and excellent operation stability in reversible solid oxide cell (SOC) modes for more than 200 h.[49] The decoration method has significant advantages over the conventional composite by mechanical mixing or infiltration techniques. Bismuth oxide based composite electrodes prepared by mechanical mixing require a high temperature pre-sintering step,[40, 46, 51] which can be detrimental to the phase and structural stability of bismuth oxide phase. The infiltration

technique avoids the high temperature sintering step, but the process is time consuming and the loading of the infiltrated phase is limited.[52] Excess infiltration also reduces the porosity and increases the diffusion resistance for the reaction.[53] Decoration methods used in this study not only avoid the high temperature sintering but also are highly flexible in the component composition without detrimental effect on the microstructure.

In this work, ESB decoration is applied to cobaltite based perovskite cathode such as Nb-doped LSCF (LSCFNb) to form an ESB decorated LSCFNb composite cathode directly assembled on YSZ electrolyte. The use of B-site doping with high valence cations like niobium is to reduce the Sr segregation and therefore increase the structural stability of LSCF.[54-55] The results indicate that there is a redistribution of ESB phase in the ESB-LSCFNb composite under polarization conditions, forming an ESB interlayer at the cathode/YSZ interface. Such formed interlayer prevents the direct contact between the segregated SrO and YSZ, resulting in the significant enhancement of the performance of LSCFNb cathode.

2. Experimental

2.1. Synthesis and fabrication of ESB decorated LSCFNb cathode and anode-supported cell

$La_{0.6}Sr_{0.4}Co_{0.2}Fe_{0.7}Nb_{0.1}O_{3-\delta}$ (LSCFNb) powder was synthesized by sol-gel method. The starting chemicals were $La(NO_3)_3{\cdot}6H_2O$ (99.9%, A.R., Alfa-Aesar), $Sr(NO_3)_2$ (99%, A.R., Sigma-Aldrich), $Co(NO_3)_2{\cdot}6H_2O$ (98-102%, A.R., Alfa-Aesar), $Fe(NO_3)_3{\cdot}9H_2O$ (98%, Sigma-Aldrich), ammonium niobate oxalate hydrate ($C_4H_4NNbO_9{\cdot}xH_2O$, 99.99%, Sigma-Aldrich), anhydrous citric acid (99.5%, A.R., Chem Supply), ethylenediaminetetraacetic acid (EDTA, 99%, Acros Organics), and ammonia solution (28%w.w., Sigma-Aldrich) with a molar ratio of 1:1.5:1(metal ions/citric acid/EDTA). The resultant gel powders were calcined at 900 °C in air for 2 h. $Er_{0.4}Bi_{1.6}O_3$ (ESB) decorated LSCFNb electrode powder with a weight percentage of 40 wt.% ESB and 60 wt.% LSCFNb was synthesized by sol-gel method. The use of 40wt%

ESB is based on the percolation limit of conductive phase in the composite.[56] ESB aqueous precursor solution consisting of $Er(NO_3)_3 \cdot 5H_2O$ (99.9%, A.R., Sigma-Aldrich), $Bi(NO_3)_3 \cdot 5H_2O$ (98%, A.R., Sigma-Aldrich), EDTA, anhydrous citric acid and ammonia was constantly stirred on a heating stage (the precursor solution will produce 4 grams of ESB powder after calcination). Then 6 grams of LSCFNb powder was added to the ESB precursor solution and stirred until the gelation starts. The resultant gel was further dried at 150^{o}C for 8 h in an oven and then calcined at 600^{o}C in air for 2h, forming ESB decorated LSCFNb powder (ESB-LSCFNb). The ESB-LSCFNb powder was mechanically blended with the ink vehicle (Fuel Cell Materials, US) with a weight ratio of 7:3 using a mortar and pestle to obtain cathode ink. LSCFNb-YSZ oxide couples with a weight ratio of 5:5 were also made and heat treated at 750, 800, 850 and 900 ^{o}C in air for 2 h.

Ni-YSZ anode-supported YSZ electrolyte cells (φ 15 mm × 0.8 mm) were prepared by spin coating method followed by co-sintering at 1450^{o}C for 5h.[57] For the anode support, NiO (J.T. Baker), 8 mol% Y_2O_3-doped ZrO_2 (YSZ, Tosoh) powder and tapioca were blended with a weight ratio of 5:5:2.5. The anode functional layer (AFL) was fabricated by mixing YSZ and NiO with a weight ratio of 5:5. The thickness of the NiO-YSZ support, AFL and YSZ film was 800, 9 and 11 μm, respectively. The LSCFNb and ESB-LSCFNb cathode pastes were directly screen-printed onto the YSZ electrolyte and then dried at 100 ^{o}C for 2 h to obtain the directly assembled LSCFNb/YSZ and ESB-LSCFNb/YSZ cells. Gold paste (Gwent Electronic Materials Ltd, UK) was painted on the electrode surface and dried at 150 ^{o}C, serving as the current collector. The cathode has a geometric area of 0.2 cm^2 with a thickness of ~19 μm. Stability test was performed at 750 ^{o}C and 250 mA cm^{-2} for 100 hrs. In order to study the influence of cathodic polarization on the electrode/electrolyte interface, an anode supported cell with directly assembled electrode was dwelled at 750 ^{o}C for 100 hrs without polarization treatment, *i.e.*, under open circuit condition.

YSZ electrolyte-supported cells were also prepared to study the electrochemical impedance behaviour of LSCFNb and ESB-LSCFNb electrodes for the oxygen reduction reaction via a three-electrode configuration.[58] YSZ electrolyte discs were fabricated by die pressing YSZ powder, followed by sintering at 1450ºC for 5 h. The thickness and diameter of the YSZ electrolyte pellet were 1.0 mm 20 mm, respectively. Platinum ink (Gwent Electronic Materials Ltd., UK) was printed at the centre and edge of the YSZ pellet as the counter and reference electrodes, followed by sintering at 1100 ºC for 2 h. Cathode paste was painted on the other side of the YSZ electrolyte, symmetrically opposite to the platinum counter electrode.

2.2. Characterization

The anode supported YSZ electrolyte cells were sealed onto Al_2O_3 tubes using a ceramic sealant (Ceramabond 552, Aremco Products Inc.). H_2 at a flow rate of 50 mL min^{-1} was supplied to the NiO-YSZ anode and the cathode was exposed to the ambient air. The NiO-YSZ anode was reduced in H_2 at 750 ºC for 1 h before the electrochemical tests. The electrochemical impedance, polarization curves and stability curves were recorded using a electrochemical workstation (Gamry Reference 3000 Potentiostat) at a temperature range of 600 -750 ºC. The electrochemical impedance was recorded in a frequency range of 100 mHz to 100 kHz with a signal amplitude of 10 mV under open circuit conditions. Electrode ohmic resistance (R_Ω) was obtained from the high frequency intercept, and electrode polarization resistance (R_p) was calculated from the differences between the high and low frequency intercepts of the impedance curves.[59] The operation stability of the cell was recorded under a constant current of 250 mA cm^{-2} at 750 ºC. In order to ensure the reproducibility, the measurements were repeated at least on two different cells. Activation energy of LSCFNb and ESB-LSCFNb cathodes for the oxygen reduction reaction was obtained from the slope of the Arrhenius plots of R_p by the impedance measurements in the temperature range of 600-800 ºC on YSZ electrolyte-supported cells.

The phases of the prepared cathode powders and the LSCFNb-YSZ oxide couple calcined at different temperatures were identified by a Bruker D8 Advance X-ray diffractometer (XRD) equipped with a copper Kα source. The microstructure of the YSZ electrolyte surface in contact with LSCFNb and ESB-LSCFNb cathodes was studied by scanning electron microscopy (SEM, Zeiss Neon 40EsB). To examine the morphology of the YSZ electrolyte surface, the electrode coating was completely removed by hydrochloric acid (HCl, 32 wt%, Sigma-Aldrich) treatment, and in some occasions, the electrode was partly peeled off to investigate the electrode/electrolyte interface. YSZ electrolyte lamella in contact with the cathode particles was prepared with a thickness of around 60 nm using a Dual Beam Focused Ion Beam - Scanning Electron Microscope (FIB-SEM, Helios Nanolab G3 CX, FEI company) with Ga^+ ion source at 30 kV. The FIB milled lamellae were examined using a high angle annular dark field scanning transmission electron microscopy (HAADF-STEM, FEI Titan G2 80-200 TEM/STEM with ChemiSTEM Technology) at 200 kV to obtain the EDS elemental mapping results and microstructural micrographs. TEM Imaging & Analysis software (TIA, FEI Company) was used to extract the fast Fourier transform (FFT) images from the TEM micrographs, in order to study the diffraction behavior of selected regions.

3. Results and Discussion

3.1. Thermal compatibility and microstructure of cathode powder and cell

Figure 1a presents the XRD pattern of the LSCFNb-YSZ oxide couples after heat treatment at 750, 800, 850 and 900ºC. XRD peaks for the pure perovskite and cubic phases were identified for the LSCFNb and YSZ oxides after the calcination at 750, 800 and 850ºC. The oxide couple started to react at 900ºC, forming $SrZrO_3$ phase. The $SrZrO_3$ (002), (040) and (042) planes were identified at 30.8 º, 44.7 º and 54.9 º.[60-61] However, in the case of LSCF-YSZ oxide couple, the reaction starts at a temperature as low as 800ºC.[62-63] This implies that the Nb

doping evidently improves the chemical compatibility between LSCFNb and YSZ. However, bismuth oxide may not be stable at temperatures of ~850 ^{o}C. Therefore, to avoid the possible decomposition and instability of ESB in the ESB-LSCFNb composite electrodes, test has been carried out at a low temperature of 750 ^{o}C in this study. The cross-section of the anode-supported YSZ electrolyte cell with ESB-LSCFNb cathode after the electrochemical tests is also shown in Figure 1b. A good contact between the porous cathode and the dense YSZ electrolyte was observed. The thickness of the electrolyte was ~10 μm. The STEM-EDS mapping showed the uniformly distributed LSCFNb nano-particles with a dimension of 154 ± 43 nm, encapsulated in the ESB network. The results indicate the successful fabrication of ESB decorated LSCFNb electrodes and directly assembled on barrier-layer-free YSZ electrolyte cell.

3.2. Electrochemical performance and microstructure of electrode/electrolyte interface

Figure 2 presents the electrochemical performance results of anode-supported YSZ electrolyte cells with directly assembled LSCFNb and ESB-LSCFNb cathodes polarized at 250 mAcm^{-2} and 750^{o}C. For the cell with ESB-LSCFNb cathode, the peak power density (PPD) is 1.32, 0.78, 0.45 and 0.24 W cm^{-2} at 750, 700, 650 and 600 ^{o}C, respectively (Figure2a). R_{Ω} of the cell is 0.07, 0.10, 0.16 and 0.27 Ω cm^2 at 750, 700, 650 and 600 ^{o}C, respectively, and R_p of the cell is 0.40, 0.68, 1.33 and 3.00 Ω cm^2 at 750, 700, 650 and 600 ^{o}C, respectively (Figure2b). As a comparison, the cell with directly assembled LSCFNb cathode was also tested. The PPD of the LSCFNb cell is 0.53 W cm^{-2} at 750^{o}C, which is much lower as compared to 1.32 W cm^{-2} acquired on the ESB-LSCFNb cell (Figure 2c). The impedance of the LSCFNb cell is also much higher than that of ESB-LSCFNb cell. For example, R_{Ω} and R_p of the LSCFNb cell are 0.29 and 0.50 Ω cm^2 at 750^{o}C, respectively, significantly larger than 0.07 and 0.32 Ω cm^2 obtained on ESB-LSCFNb cells under identical test conditions. R_p of LSCFNb cell is also larger than 0.27 Ω cm^2 for the cell with directly assembled LSCF cathode under similar test conditions.[55] This indicates that Nb doping reduces the electrocatalytic activity of LSCF

electrode for ORR, in good agreement with that reported on Nb-doped $Ba_{0.5}Sr_{0.5}Co_{0.8}Fe_{0.2}O_{3-\delta}$ (BSCF) membranes.[64]

The low polarization resistance of the cell with ESB-LSCFNb cathode is clearly due to the much higher electrocatalytic activity of the ESB-LSCFNb electrode for ORR. As shown in Figure 2e, R_p of the ESB-LSCFNb composite cathode on YSZ electrolyte supported cell is 7.2 Ω cm^2 at 600 ^{o}C, which is significantly smaller than 55.2 Ω cm^2 obtained on LSCFNb cathode. Most importantly, activation energy of R_p for the ORR on the ESB-LSCFNb composite electrode is 98 kJ mol^{-1}, substantially lower than 214 kJ mol^{-1} acquired on LSCFNb electrode (Figure 2f). The results indicate that the ESB decoration significantly reduces the activation energy and improves the electrocatalytic activity of the electrode for ORR. This implies that decorated ESB is most effective to enhance the activity of LSCF-based cathode at reduced temperatures. The ESB-LSCFNb cell was stable with negligible change in the cell voltage after polarization at 750 ^{o}C and 250 mAcm^{-2} for 100 hrs (Figure 2g). The initial cell voltage was 0.96 V and slightly decreased to 0.90 V after cathodic polarization for 100 hrs. However, different from that of ESB-LSCFNb cell, the cell with LSCFNb cathode was not stable and the cell voltage decreased rather significantly from 0.87 V to 0.72 V under similar testing conditions (Figure 2h).

The morphology of YSZ electrolyte surface in contact with directly assembled LSCFNb and ESB-LSCFNb cathodes is shown in Figure 3. The cathodes were either peeled off using adhesive tape (Figure 3b,d,f) or removed by acid treatment (Figure 3a,c,e). The YSZ surface in contact with LSCFNb cathode was characterized by the formation of large number of ring-shaped contact craters with a dimension of 0.34 ± 0.15 μm (inset in Figure 3a). As shown in Figure 3b, a large number of island structure were observed after the LSCFNb cathode was peeled off using sticky tape. These islands have a dimension of 0.53 ± 0.25 μm, which is close to that of the ring-shaped craters observed on the electrolyte. The change in the surface

morphology of the YSZ electrolyte clearly indicates the significant interaction between LSCFNb cathode and YSZ electrolyte during the cathodic polarization. In contrast, in the case of the ESB-LSCFNb cell, the YSZ electrolyte surface was reasonably smooth and flat after the cathodic polarization at 750 ^{o}C and 250 mA cm^{-2} for 100 hrs, and the size of ring-shaped contact craters was much smaller (0.17 ± 0.15 μm) (Figure 3c), as compared to that on YSZ surface in contact with LSCFNb cathode (Figure 3a). There was also formation of island structures on the YSZ surface but different to that observed on the YSZ electrolyte surface of the LSCFNb cell, the islands appear to consist of small particles deposited on a plate-like layer with size in the range of 0.77 ± 0.44 μm (Figure 3d), substantially larger than that of the ring-shaped contact craters. Without cathodic polarization, the YSZ surface in contact with ESB-LSCFNb cathode was smooth and no contact marks were observed (Figure3e), indicating that no reactions occurred between ESB-LSCFNb cathode and YSZ electrolyte at 750 ^{o}C under open circuit conditions. The particles left on the YSZ electrolyte surface after the cathode coating was removed by adhesive tape were ESB-LSCFNb cathode particles (Figure 3f). The morphology of the ESB-LSCFNb composite cathode particles is similar to the as-synthesized ESB-LSCFNb powder as shown in Figure 1c. This indicates again that the ring-shaped contact craters observed on YSZ electrolyte surface in contact with LSCFNb and ESB-LSCFNb cathode are induced by the cathodic polarization treatment.

3.3. LSCFNb/YSZ interface

Figure 4 presents the HAADF micrograph and STEM-EDS element mapping of the LSCFNb/YSZ interface region of a directly assembled LSCFNb cell after cathodic polarization at 250 mA cm^{-2} and 750^{o}C for 100 hrs. A thick layer (~100 nm) with different contrast to that of dense YSZ electrolyte and porous LSCFNb cathode was observed between the cathode and electrolyte. The size of this reaction phase was 0.54 μm, similar to the size of island structures (0.53 ± 0.25 μm) observed in Figure 3b. The originally flat YSZ surface became curved

(indicated by arrow in Figure 4a), corresponding to the ring-shaped convex contact craters (see Figure 3a). The mapping results clearly identified the LSCFNb cathode and YSZ electrolyte. For the reaction layer at the cathode/electrolyte interface, a strong accumulation of Sr and Zr was detected. This implies the possible formation of $SrZrO_3$ layer under the influence of cathodic polarization, similar to that observed for the directly assembled LSCF cathode on YSZ electrolyte.[63] The accumulation of Sr at the interface region implies the substantial Sr segregation and diffusion under cathodic polarization conditions, in good agreement with that reported in the literature.[65-67] Different to the conventional chemical reaction between two phases, such surface segregation induced chemical reaction can occur at a much lower temperature. Yung *et al*. observed the chemical reaction between BSCF cathode and $Ce_{0.8}Sm_{0.2}O_{1.95}$ and $Ce_{0.9}Gd_{0.1}O_{1.95}$ electrolytes at 700 ^oC under the influence of cathodic polarization.[68] Without the influence of polarization, such reaction only occurs at 900 ^oC. The reaction has been attributed to the Ba segregation induced by cathodic polarization.

The reaction layer at the electrode/electrolyte interface of the directly assembled LSCFNb cell was examined by FIB-STEM (Figure 4b). The reaction layer has an intimate contact with the YSZ electrolyte. The $\{103\}_{SrZrO3}$ lattice planes with a plane spacing of 0.18 nm indicate the formation of $SrZrO_3$ phase in the reaction layer, while the YSZ phase was identified by the $\{200\}_{YSZ}$ planes with plane spacing of 0.25 nm. The FFT image of YSZ phase shows a typical cubic structure, taken along $[001]_{YSZ}$ zone axis.[69] In this case, the $\{200\}_{YSZ}$ and $\{103\}_{SrZrO3}$ lattice planes meet at the interface with the corresponding orientation relationship, $\theta_{\{103\}SrZrO3/\{200\}YSZ}$ of 44.7^o and a mismatch factor (*f*) of 28.0%. The occurrence of the lattice plane distortion was observed in the interface region. The lattice distortion is widely observed for hetero-interfaces, in order to accommodate the lattice mismatch between two different phases.[70-72] This study indicates the substantial Sr segregation of Nb doped LSCF (LSCFNb), different from the suppressed Sr segregation reported on Nb-doped cobaltite perovskite cathode

on GDC electrolyte.[54, 73] The reason may be related to the direct contact between the SrO and YSZ electrolyte, which leads to the formation of $SrZrO_3$ and in turn accelerates the Sr segregation.

3.4. ESB-LSCFNb/YSZ interface

Figure 5 shows the HAADF micrograph and STEM-EDS mapping of the cathode/electrolyte interface of a directly assembled ESB-LSCFNb cell after cathodic polarization at 250 $mAcm^{-2}$ and 750^{o}C for 100 hrs. Very different from that observed on the LSCFNb cell, the YSZ surface was flat and no curvature on the electrolyte surface in contact with ESB-LSCFNb electrode was observed, indicating a very stable interface between ESB-LSCFNb cathode and YSZ electrolyte even after the cathodic polarization at 250 $mAcm^{-2}$ and 750 ^{o}C for 100 hrs. Except individual and isolated Sr-rich areas/particles with size in the range of 10-40 nm, La and other elements of LSCFNb (not shown for clarity of the data) were uniformly distributed, indicating that Sr segregation and diffusion of LSCFNb electrode under polarization conditions are significantly suppressed by the ESB decoration. In contrast to the uniform distribution and network of bismuth in the original ESB decorated LSCFNb powders (see Figure1c), there was almost no bismuth present in the LSCFNb particles at the cathode/electrolyte interface. Instead, there was a clear accumulation and enrichment of Bi on the electrolyte surface between YSZ and LSCFNb particles. The Bi layer is not uniform and appears to fill the open space on the electrolyte surface between the LSCFNb particles. The thickness of this bismuth oxide layer varies significantly between a few nm to 100-200 nm. The remarkable change in the distribution of Bi and its migration at the interface region in the ESB-LSCFNb cell evidently occurred under the influence of the cathodic polarization. The clear boundary between bismuth oxide and LSCFNb phase also indicates no chemical reaction between LSCFNb and ESB. No Zr was observed in the ESB-LSCFNb cathode, indicating that there is no cation interdiffusion between YSZ electrolyte and ESB-LSCFNb electrode. The diffusion and accumulation of

bismuth at the interface was also observed on the bismuth oxide decorated $Sm_{0.96}Co_{0.95}Pd_{0.05}O_{3-\delta}$ oxygen electrodes of reversible solid oxide cells after polarization at 500 mA cm^{-2} and 750 ^{o}C for 500 hrs.[50]

The microstructure of the accumulated bismuth layer on the electrolyte surface was examined by HRTEM, taken along $[011]_{ESB}$ zone axis (Figure 5b). The migrated ESB phase has established an intimate contact with the YSZ electrolyte, and the ESB/YSZ interface was very sharp and abrupt as a result of their similar intrinsic cubic structure with space group symmetry of Fm-3m and lattice constants of 5.48 Å and 5.13 Å, respectively.[74-75] From the interface region, the $\{111\}_{YSZ}$ lattice planes with a plane spacing of 0.29 nm and the $\{111\}_{ESB}$ lattice planes with a plane spacing of 0.33 nm are associated with YSZ and ESB phases, respectively. The $\{111\}_{YSZ}$ and $\{111\}_{ESB}$ planes meet and match at the interface, with orientation relationship of 9.4^{o} and mismatch factor of 12.1%. Lattice distortion for the two phases was also observed around the interface, but no additional or amorphous phases were found at the ESB/YSZ interface. The formation of an ESB layer at the interface would act as a barrier layer, preventing the direct contact and subsequent reactions between the segregated SrO and YSZ electrolyte. This explains the high performance and stability of the ESB-LSCFNb cells tested at 750 ^{o}C and 250 mAcm^{-2} for 100 hrs (Figure2).

In order to confirm the *in situ* formation of ESB interlayer on YSZ electrolyte induced under the influence of cathodic polarization, an anode supported cell with directly assembled ESB-LSCFNb electrode was prepared. Figure 6 presents the HAADF micrograph and STEM-EDS element mapping results for the cathode/electrolyte interface of the as-prepared ESB-LSCFNb cell after dwell at 750 ^{o}C for 100 hrs with no polarization. LSCFNb particles were identified with size of 129 ± 72 nm. ESB phase was characterized by fine and needle-like particles, probably due to dwell at 750 ^{o}C for 100 hrs, and uniformly distributed between LSCFNb particles, similar to the as-synthesized ESB-LSCFNb composite powder (Figure 1c). No

specific accumulation or diffusion of bismuth toward the YSZ electrolyte surface was observed. This evidently indicates that the re-distribution and migration of ESB phase toward YSZ electrolyte does not occur at 750 ^{o}C under open circuit conditions. This in turn demonstrates that decorated ESB phase comes out of the ESB-LSCFNb composite and is driven to the YSZ electrolyte under the influence of cathodic polarization conditions, forming a bismuth interlayer at the LSCFNb cathode/YSZ electrolyte interface region (see Figure 5).

3.5. Effects of polarization on Sr segregation and ESB-LSCFNb/YSZ interface formation

The results of the present study clearly demonstrate the influence of cathodic polarization on the Sr segregation and electrode/electrolyte interface formation for LSCFNb/YSZ and ESB-LSCFNb/YSZ cells. In the case of LSCFNb/YSZ cell, a significant Sr segregation and diffusion was observed on the electrolyte surface, leading to the formation of ring-shaped contact craters on the electrolyte surface. The segregated SrO is highly mobile [5, 76-77] and reacts with YSZ, forming a thick layer of $SrZrO_3$, similar to that observed in LSCF/YSZ cell.[67] This in turn indicates that the direct contact between segregated SrO and YSZ accelerates the Sr segregation despite the Nb doping at the B-site of LSCF.

In the case of ESB-LSCFNb/YSZ cell, ESB decoration significantly improves the electrocatalytic activity and stability of the LSCFNb cathode. The anode supported YSZ electrolyte cell with ESB-LSCFNb cathode exhibits a much higher PPD (1.32 W cm^{-2}) than that of LSCFNb cell (0.53 W cm^{-2}) at 750^{o}C. In contrast to the LSCFNb cell, the YSZ surface in contact with ESB-LSCFNb electrode is very stable. The stable interface is clearly due to the redistribution and diffusion of the ESB phase, forming a bismuth oxide layer at the cathode/electrolyte interface under the influence of cathodic polarization, as shown in Figure 5. The migration of bismuth oxide phase was also reported by others.[78-79] Lee *et al.*[78] prepared the ESB-LSM composite cathode by a conjugated reverse-strike co-precipitation and glycine-

nitrate combustion method and observed the formation of a continuous nano-scale ESB layer (~50 nm) at the electrode/YSZ electrolyte interface after polarization test. The formation of thin ESB layer was attributed to its high wettability and mobility due to the low melting temperature of bismuth oxide (~827ºC). Fan *et al*.[79] also observed a dense Bi_2O_3-LSCF film at the electrode/electrolyte interface on 1 mol% Bi_2O_3-LSCF composite electrode after polarization and proposed that the addition of Bi_2O_3 into LSCF promoted the formation of eutectic liquid, which flows down to the electrolyte surface to form a dense layer. In the present study, the HAADF and STEM-EDS element mapping of the cathode/electrolyte interface of anode supported YSZ electrolyte cells with ESB-LSCFNb cathodes before and after polarization evidently demonstrates that ESB is separated from the mixed ESB-LSCFNb phase and migrates to the electrolyte surface, forming an interlayer at the electrode/YSZ electrolyte interface. The formed interlayer is irregular in shape and much thicker than that observed by Lee et al on ESB/LSM cathode/YSZ electrolyte interface.[78] This indicates the high mobility of the decorated ESB phase under the SOFC operating conditions. The possible formation of eutectic phase with LSCFNb can be ruled out as no LSCFNb elements were observed in the ESB layer at the interface (see Figure5a). The presence of the highly oxygen ionic conducting ESB layer at the interface not only improves the electrocatalytic activity of the LSCFNb cathode, but also promotes the rapid ion migration at the electrode/electrolyte interface.[49, 78] The *in situ* formed ESB layer acts as a barrier layer to prevent the reaction between the segregated SrO and YSZ, inhibiting the formation of $SrZrO_3$ at the cathode/electrolyte interface and thus preventing the further segregation of Sr (Figure 5a). Figure 7 shows the schematic diagram of the fabrication of ESB-LSCFNb electrode via decoration method and the *in situ* formation of ESB layer at the cathode/electrolyte interface region under the influence of cathodic polarization.

In general, direct addition of ESB interlayer between electrolyte and cathode would require high temperature sintering to form the strong adhesion between the ESB interface and electrolyte before the application of the cathode. However, due to the low decomposition temperature, pre-sintering of ESB interlayer may not be feasible. As shown in this study, ESB functional layer is formed *in situ* under the influence of polarization at operation temperatures of 750^{o}C, which is below the decomposition temperature of bismuth oxide. The *in situ* formation of the ESB functional layer occurs under normal operation conditions and does not require additional cell fabrication procedures. This also greatly simplifies the manufacturing process and thus reduces the cost of SOFCs.

4. Conclusions

The ESB decorated LSCFNb nanostructured cathode powder was successfully fabricated in the present study and the influence of ESB decoration on the electrochemical performance, electrode/electrolyte interface formation and Sr segregation of the LSCFNb/YSZ cell was investigated in detail *via*. combined FIB-STEM technique. The results show evidently that the cell with the directly assembled ESB-LSCFNb electrode exhibits a much higher peak power density, 1.32 W cm^{-2} at 750 ^{o}C as compared to the 0.53 W cm^{-2} for the cell with LSCFNb electrode. The ESB-LSCFNb/YSZ cell also shows excellent stability under the cathodic polarization at 750 ^{o}C and 250 mA cm^{-2} for 100 hrs. In the case of the directly assembled LSCFNb/YSZ cell, there is significant reaction between the segregated SrO and YSZ electrolyte, forming a thick $SrZrO_3$ layer between LSCFNb electrode and YSZ electrolyte and characterized by the formation of ring-shaped convex craters on the electrolyte surface. On the other hand, in the ESB-LSCFNb/YSZ cell, the decorated nano-scaled ESB comes out of the ESB-LSCFNb composite and deposits at the cathode/electrolyte interface. The fundamental reason for its high wettability and mobility is most likely due to the low melting temperature of bismuth oxide (~827^{o}C).

The *in situ* formed ESB layer functions as barrier layer to prevent the direct contact and interaction between the segregated SrO and YSZ and promotes the ORR of the LSCFNb electrode. The significantly reduced activation energy for the ORR on ESB-LSCFNb cathode implies that ESB decoration is most effective for the enhancement of the electrocatalytic activity at reduced temperatures. The present study clearly demonstrates the dynamic relationship between interface, segregation, and performance of bismuth oxide decorated electrode materials for fuel cells. The *in situ* formation of highly active and functional ESB interlayer demonstrated the promising potential of the approach for the development in intermediate temperature SOFCs.

Author information

Corresponding author: *E-mail: s.jiang@curtin.edu.au

Notes:

The authors declare no competing financial interest.

Acknowledgment

This work was financially supported by the Australian Research Council under the Discovery Project Scheme (project number: DP150102025, DP150102044, DP180100731 and DP180100568) and the Chinese Scholarship Council. The authors acknowledge the facilities and the scientific and technical assistance of Curtin University Microscopy & Microanalysis Facility and the Australian Microscopy & Microanalysis Research Facility at the Centre for Microscopy, Characterization & Analysis, The University of Western Australia, a facility funded by the University, State and Commonwealth Governments.

References:

1. Wachsman, E. D.; Lee, K. T., Lowering the Temperature of Solid Oxide Fuel Cells. *Science* **2011,** *334*, 935-939.
2. Gur, T. M., Comprehensive Review of Methane Conversion in Solid Oxide Fuel Cells: Prospects for Efficient Electricity Generation from Natural Gas. *Prog. Energy Combust. Sci.* **2016,** *54*, 1-64.
3. Wang, S. Y.; Jiang, S. P., Prospects of Fuel Cell Technologies. *National Sci. Rev.* **2017,** *4*, 163-166.
4. Choudhury, A.; Chandra, H.; Arora, A., Application of Solid Oxide Fuel Cell Technology for Power Generation-a Review. *Renew. Sust. Energ. Rev.* **2013,** *20*, 430-442.
5. Kiebach, R.; Zhang, W.-W.; Zhang, W.; Chen, M.; Norrman, K.; Wang, H.-J.; Bowen, J. R.; Barfod, R.; Hendriksen, P. V., Stability of $La_{0.6}Sr_{0.4}Co_{0.2}Fe_{0.8}O_3/Ce_{0.9}Gd_{0.1}O_2$ Cathodes During Sintering and Solid Oxide Fuel Cell Operation. *J. Power Sources* **2015,** *283*, 151-161.
6. Jiang, S. P., Sintering Behavior of Ni/Y2o3-Zro2 Cermet Electrodes of Solid Oxide Fuel Cells. *J. Mater. Sci.* **2003,** *38*, 3775-3782.
7. Jiang, S. P.; Chan, S. H., A Review of Anode Materials Development in Solid Oxide Fuel Cells. *J. Mater. Sci.* **2004,** *39*, 4405-4439.
8. Liu, Y. L.; Hagen, A.; Barfod, R.; Chen, M.; Wang, H. J.; Poulsen, F. W.; Hendriksen, P. V., Microstructural Studies on Degradation of Interface between Lsm–Ysz Cathode and Ysz Electrolyte in Sofcs. *Solid State Ionics* **2009,** *180*, 1298-1304.
9. Jiang, S. P.; Zhang, J. P.; Foger, K., Chemical Interactions between 3 Mol% Yttria-Zirconia and Sr-Doped Lanthanum Manganite. *J. Eur. Ceram. Soc.* **2003,** *23*, 1865-1873.
10. Jiang, S. P.; Chen, X. B., Chromium Deposition and Poisoning of Cathodes of Solid Oxide Fuel Cells - a Review. *Int. J. Hydrog. Energy* **2014,** *39*, 505-531.
11. De Vero, J. C.; Develos-Bagarinao, K.; Liu, S. S.; Kishimoto, H.; Ishiyama, T.; Yamaji, K.; Horita, T.; Yokokawa, H., Sulfur Poisoning Behavior of La1-Xsrxco1-Yfeyo3-Delta Thin Films with Different Compositions. *J. Alloy. Compd.* **2018,** *748*, 608-619.
12. Lee, H. Y.; Oh, S. M., Origin of Cathodic Degradation and New Phase Formation at the La0.9sr0.1mno3/Ysz Interface. *Solid State Ionics* **1996,** *90*, 133-140.
13. Mitterdorfer, A.; Gauckler, L. J., La2zr2o7 Formation and Oxygen Reduction Kinetics of the La0.85sr0.15mnyo3, O2(G)|Ysz System. *Solid State Ionics* **1998,** *111*, 185-218.
14. Yokokawa, H., Understanding Materials Compatibility. *Ann. Rev. Mater. Res.* **2003,** *33*, 581-610.
15. Menzler, N. H.; Tietz, F.; Uhlenbruck, S.; Buchkremer, H. P.; Stover, D., Materials and Manufacturing Technologies for Solid Oxide Fuel Cells. *J. Mater. Sci.* **2010,** *45*, 3109-3135.
16. Brett, D. J. L.; Atkinson, A.; Brandon, N. P.; Skinner, S. J., Intermediate Temperature Solid Oxide Fuel Cells. *Chem. Soc. Rev.* **2008,** *37*, 1568-1578.
17. Adler, S. B., Factors Governing Oxygen Reduction in Solid Oxide Fuel Cell Cathodes. *Chem. Rev.* **2004,** *104*, 4791-4843.
18. Mineshige, A.; Izutsu, J.; Nakamura, M.; Nigaki, K.; Abe, J.; Kobune, M.; Fujii, S.; Yazawa, T., Introduction of a-Site Deficiency into La0.6sr0.4co0.2fe0.8o3–Δ and Its Effect on Structure and Conductivity. *Solid State Ionics* **2005,** *176*, 1145-1149.
19. S. Carter; A. Selcuk; R.J. Chater; J. Kajda; Kilner, J. A.; Steele, a. B. C. H., Oxygen Transport in Selected Nonstoichiometric Perovskite-Structure Oxides. *Solid State Ionics* **1992,** *53-56*, 597-605.
20. Teraoka, Y.; Nobunaga, T.; Okamoto, K.; Miura, N.; Yamazoe, N., Influence of Constituent Metal Cations in Substituted Lacoo3 on Mixed Conductivity and Oxygen Permeability. *Solid State Ionics* **1991,** *48*, 207-212.
21. Perry Murray, E., Electrochemical Performance of (La,Sr)(Co,Fe)O3–(Ce,Gd)O3 Composite Cathodes. *Solid State Ionics* **2002,** *148*, 27-34.

22. Haider, M. A.; McIntosh, S., The Influence of Grain Size on La0.6sr0.4co0.2fe0.8o3-Δ Thin Film Electrode Impedance. *J. Electrochem. Soc.* **2011,** *158*, B1128-B1136.
23. Sun, C.; Hui, R.; Roller, J., Cathode Materials for Solid Oxide Fuel Cells: A Review. *J. Solid State Electrochem.* **2009,** *14*, 1125-1144.
24. Baharuddin, N. A.; Rahman, H. A.; Muchtar, A.; Sulong, A. B.; Abdullah, H., Development of Lanthanum Strontium Cobalt Ferrite Composite Cathodes for Intermediate- to Low-Temperature Solid Oxide Fuel Cells. *J. Zhejiang Univ. SCI. A* **2013,** *14*, 11-24.
25. Bucher, E.; Sitte, W., Long-Term Stability of the Oxygen Exchange Properties of (La,Sr)1−Z(Co,Fe)O3−Δ in Dry and Wet Atmospheres. *Solid State Ionics* **2011,** *192*, 480-482.
26. Esquirol, A.; Brandon, N. P.; Kilner, J. A.; Mogensen, M., Electrochemical Characterization of La0.6sr0.4co0.2fe0.8o3 Cathodes for Intermediate-Temperature Sofcs. *J. Electrochem. Soc.* **2004,** *151*, A1847-A1855.
27. Chen, J.; Liang, F. L.; Chi, B.; Pu, J.; Jiang, S. P.; Jian, L., Palladium and Ceria Infiltrated La0.8sr0.2co0.5fe0.5o3-Delta Cathodes of Solid Oxide Fuel Cells. *J. Power Sources* **2009,** *194*, 275-280.
28. Jiang, S. P., A Comparison of O-2 Reduction Reactions on Porous (La,Sr)Mno3 and (La,Sr)(Co,Fe)O-3 Electrodes. *Solid State Ionics* **2002,** *146*, 1-22.
29. Singh, B.; Ghosh, S.; Aich, S.; Roy, B., Low Temperature Solid Oxide Electrolytes (Lt-Soe): A Review. *J. Power Sources* **2017,** *339*, 103-135.
30. Zhang, Y.; Knibbe, R.; Sunarso, J.; Zhong, Y.; Zhou, W.; Shao, Z.; Zhu, Z., Recent Progress on Advanced Materials for Solid-Oxide Fuel Cells Operating Below 500 Degrees C. *Adv Mater* **2017**.
31. Li, M.; Zhao, M.; Li, F.; Zhou, W.; Peterson, V. K.; Xu, X.; Shao, Z.; Gentle, I.; Zhu, Z., A Niobium and Tantalum Co-Doped Perovskite Cathode for Solid Oxide Fuel Cells Operating Below 500 Degrees C. *Nat Commun* **2017,** *8*, 13990.
32. Zhu, Y.; Zhou, W.; Ran, R.; Chen, Y.; Shao, Z.; Liu, M., Promotion of Oxygen Reduction by Exsolved Silver Nanoparticles on a Perovskite Scaffold for Low-Temperature Solid Oxide Fuel Cells. *Nano Lett* **2016,** *16*, 512-8.
33. Duan, C.; Hook, D.; Chen, Y.; Tong, J.; O'Hayre, R., Zr and Y Co-Doped Perovskite as a Stable, High Performance Cathode for Solid Oxide Fuel Cells Operating Below 500 °C. *Energy & Environ. Sci.* **2017,** *10*, 176-182.
34. Yoo, C.-Y.; Boukamp, B. A.; Bouwmeester, H. J. M., Oxygen Surface Exchange Kinetics of Erbia-Stabilized Bismuth Oxide. *J. Solid State Electrochem.* **2010,** *15*, 231-236.
35. N. M. Sammes; G. A. Tompsett; H. Nafe; Aldinger, F., Bismuth Based Oxide Electrolytes - Structure and Ionic Conductivity. *J. Euro. Ceram. Soc.* **1999,** *19*, 1801-1826.
36. Jung, D. W.; Duncan, K. L.; Wachsman, E. D., Effect of Total Dopant Concentration and Dopant Ratio on Conductivity of (Dyo1.5)(X)-(Wo3)(Y)-(Bio1.5)1-X-Y. *Acta Mater.* **2010,** *58*, 355-363.
37. Jung, D. W.; Nino, J. C.; Duncan, K. L.; Bishop, S. R.; Wachsman, E. D., Enhanced Long-Term Stability of Bismuth Oxide-Based Electrolytes for Operation at 500 a Degrees C. *Ionics* **2010,** *16*, 97-103.
38. Joh, D. W.; Park, J. H.; Kim, D.; Wachsman, E. D.; Lee, K. T., Functionally Graded Bismuth Oxide/Zirconia Bilayer Electrolytes for High-Performance Intermediate-Temperature Solid Oxide Fuel Cells (It-Sofcs). *ACS Appl Mater Interfaces* **2017,** *9*, 8443-8449.
39. Ahn, J. S.; Camaratta, M. A.; Pergolesi, D.; Lee, K. T.; Yoon, H.; Lee, B. W.; Jung, D. W.; Traversa, E.; Wachsman, E. D., Development of High Performance Ceria/Bismuth Oxide Bilayered Electrolyte Sofcs for Lower Temperature Operation. *J. Electrochem. Soc.* **2010,** *157*, B376-B382.
40. Painter, A. S.; Huang, Y.-L.; Wachsman, E. D., Durability of (La 0.8 Sr 0.2) 0.95 Mno 3-Δ -(Er 0.2 Bi 0.8) 2 O 3 Composite Cathodes for Low Temperature Sofcs. *J. Power Sources* **2017,** *360*, 391-398.
41. Jiang, Z. Y.; Lei, Z. W.; Ding, B.; Xia, C. R.; Zhao, F.; Chen, F. L., Electrochemical Characteristics of Solid Oxide Fuel Cell Cathodes Prepared by Infiltrating (La,Sr)Mno3 Nanoparticles into Yttria-Stabilized Bismuth Oxide Backbones. *Int. J. Hydrog. Energy* **2010,** *35*, 8322-8330.

42. Hou, J.; Bi, L.; Qian, J.; Gong, Z.; Zhu, Z.; Liu, W., A Novel Composite Cathode Er 0.4 Bi 1.6 O 3 –Pr 0.5 Ba 0.5 Mno 3−Δ for Ceria-Bismuth Bilayer Electrolyte High Performance Low Temperature Solid Oxide Fuel Cells. *J. Power Sources* **2016,** *301*, 306-311.
43. Huang, S.; Zhou, G.; Xie, Y., Electrochemical Performances of Ag–(Bi2o3)0.75(Y2o3)0.25 Composite Cathodes. *J. Alloy. Compd.* **2008,** *464*, 322-326.
44. Camaratta, M.; Wachsman, a. E. D., Ag-Bi1. 6er0. 4o3 as a Potential Cathode Material for It-Sofcs. *ECS Transactions* **2006,** *1*, 279-292.
45. Jaiswal, A.; Hu, C. T.; Wachsman, E. D., Bismuth Ruthenate-Stabilized Bismuth Oxide Composite Cathodes for It-Sofc. *J. Electrochem. Soc.* **2007,** *154*, B1088-B1094.
46. Lee, K. T.; Jung, D. W.; Yoon, H. S.; Lidie, A. A.; Camaratta, M. A.; Wachsman, E. D., Interfacial Modification of La0.80sr0.20mno3−Δ–Er0.4bi0.6o3 Cathodes for High Performance Lower Temperature Solid Oxide Fuel Cells. *J. Power Sources* **2012,** *220*, 324-330.
47. Kharton, V.; Naumovich, E.; Samokhval, V., Formation and Properties of Reaction Layers of Cobaltite Electrodes on Bismuth Oxide Electrolytes. *Solid State Ionics* **1997,** *99*, 269-280.
48. Li, G.; He, B.; Ling, Y.; Xu, J.; Zhao, L., Highly Active Ysb Infiltrated Lscf Cathode for Proton Conducting Solid Oxide Fuel Cells. *Int. J. Hydrog. Energy* **2015,** *40*, 13576-13582.
49. Ai, N.; Li, N.; He, S.; Cheng, Y.; Saunders, M.; Chen, K.; Zhang, T.; Jiang, S. P., Highly Active and Stable Er0.4bi1.6o3 Decorated La0.76sr0.19mno3+Δ Nanostructured Oxygen Electrodes for Reversible Solid Oxide Cells. *J. Mater. Chem. A* **2017,** *5*, 12149-12157.
50. Ai, N.; Chen, M.; He, S.; Chen, K.; Zhang, T.; Jiang, S. P., High Performance Nanostructured Bismuth Oxide–Cobaltite as a Durable Oxygen Electrode for Reversible Solid Oxide Cells. *J. Mater. Chem. A* **2018,** *6*, 6510-6520.
51. Li, J.; Wang, S.; Sun, X.; Liu, R.; Ye, X.; Wen, Z., Improvement of (La0.74bi0.10sr0.16)Mno3–Bi1.4er0.6o3 Composite Cathodes for Intermediate-Temperature Solid Oxide Fuel Cells. *J. Power Sources* **2008,** *185*, 649-655.
52. Jiang, S. P., Nanoscale and Nano-Structured Electrodes of Solid Oxide Fuel Cells by Infiltration: Advances and Challenges. *Int. J. Hydrog. Energy* **2012,** *37*, 449-470.
53. Jiang, S. P.; Duan, Y. Y.; Love, J. G., Fabrication of High-Performance Nioy2o3-Zro2 Cermet Anodes of Solid Oxide Fuel Cells by Ion Impregnation. *J. Electrochem. Soc.* **2002,** *149*, A1175-A1183.
54. Chen, X. B.; Jiang, S. P., Highly Active and Stable (La0.24sr0.16ba0.6)(Co0.5fe0.44nb0.06)O3-Delta (Lsbcfn) Cathodes for Solid Oxide Fuel Cells Prepared by a Novel Mixing Synthesis Method. *J. Mater. Chem. A* **2013,** *1*, 4871-4878.
55. Chen, K. F.; He, S.; Li, N.; Cheng, Y.; Ai, N.; Chen, M. L.; Rickard, W. D. A.; Zhang, T.; Jiang, S. P., Nb and Pd Co-Doped $La_{0.57}Sr_{0.38}Co_{0.19}Fe_{0.665}Nb_{0.095}Pd_{0.05}O_{3-\delta}$ as a Stable, High Performance Electrode for Barrier-Layer-Free Y2o3-Zro2 Electrolyte of Solid Oxide Fuel Cells. *J. Power Sources* **2018,** *378*, 433-442.
56. Zhen, Y. D.; Jiang, S. P., Transition Behavior for O-2 Reduction Reaction on (La,Sr)Mno3/Ysz Composite Cathodes of Solid Oxide Fuel Cells. *J. Electrochem. Soc.* **2006,** *153*, A2245-A2254.
57. Chen, K.; Chen, X.; Lü, Z.; Ai, N.; Huang, X.; Su, W., Performance of an Anode-Supported Sofc with Anode Functional Layers. *Electrochim. Acta* **2008,** *53*, 7825-7830.
58. Jiang, S. P., Placement of Reference Electrode, Electrolyte Thickness and Three-Electrode Cell Configuration in Solid Oxide Fuel Cells: A Brief Review and Update on Experimental Approach. *J. Electrochem. Soc.* **2017,** *164*, F834-F844.
59. Li, N.; Ai, N.; Chen, K.; Cheng, Y.; He, S.; Saunders, M.; Dodd, A.; Suvorova, A.; Jiang, S. P., In Situ Assembled La0.8sr0.2mno3 Cathodes on a Y2o3–Zro2 Electrolyte of Solid Oxide Fuel Cells – Interface and Electrochemical Activity. *RSC Adv.* **2016,** *6*, 99211-99219.
60. Hasegawa, S.; Sugimoto, T.; Hashimoto, T., Investigation of Structural Phase Transition Behavior of Srzro3 by Thermal Analyses and High-Temperature X-Ray Diffraction. *Solid State Ionics* **2010,** *181*, 1091-1097.
61. Matsuda, T.; Yamanaka, S.; Kurosaki, K.; Kobayashi, S., High Temperature Phase Transitions of Srzro3. *J. Alloy. Compd.* **2003,** *351*, 43-46.

62. Mai, A.; Becker, M.; Assenmacher, W.; Tietz, F.; Hathiramani, D.; Iverstiffee, E.; Stover, D.; Mader, W., Time-Dependent Performance of Mixed-Conducting Sofc Cathodes. *Solid State Ionics* **2006,** *177*, 1965-1968.
63. Chen, K.; Li, N.; Ai, N.; Cheng, Y.; Rickard, W. D.; Jiang, S. P., Polarization-Induced Interface and Sr Segregation of in Situ Assembled $La_{0.6}Sr_{0.4}Co_{0.2}Fe_{0.8}O_{3-\delta}$ Electrodes on Y_2O_3-ZrO_2 Electrolyte of Solid Oxide Fuel Cells. *ACS Appl Mater Interfaces* **2016,** *8*, 31729-31737.
64. Fang, S. M.; Yoo, C. Y.; Bouwmeester, H. J. M., Performance and Stability of Niobium-Substituted Ba0.5sr0.5co0.8fe0.2o3-Delta Membranes. *Solid State Ionics* **2011,** *195*, 1-6.
65. Vovk, G.; Chen, X.; Mims, C. A., In Situ Xps Studies of Perovskite Oxide Surfaces under Electrochemical Polarization. *J Phys Chem B* **2005,** *109*, 2445-2454.
66. Mutoro, E.; Crumlin, E. J.; Pöpke, H.; Luerssen, B.; Amati, M.; Abyaneh, M. K.; Biegalski, M. D.; Christen, H. M.; Gregoratti, L.; Janek, J.; Shao-Horn, Y., Reversible Compositional Control of Oxide Surfaces by Electrochemical Potentials. *J. Phys. Chem. Lett.* **2012,** *3*, 40-44.
67. He, S.; Saunders, M.; Chen, K.; Gao, H.; Suvorova, A.; Rickard, W. D. A.; Quadir, Z.; Cui, C. Q.; Jiang, S. P., A Fib-Stem Study of Strontium Segregation and Interface Formation of Directly Assembled La0.6sr0.4co0.2fe0.8o3-Δ Cathode on Y2o3-Zro2 Electrolyte of Solid Oxide Fuel Cells. *J. Electrochem. Soc.* **2018,** *165*, F417-F429.
68. Yung, H.; Jian, L.; Jiang, S. P., Polarization Promoted Chemical Reaction between Ba0.5sr0.5co0.8fe0.2o3- Cathode and Ceria Based Electrolytes of Solid Oxide Fuel Cells. *J. Electrochem. Soc.* **2012,** *159*, F794-F798.
69. Wang, C. M.; Azad, S.; Shutthanandan, V.; McCready, D. E.; Peden, C. H. F.; Saraf, L.; Thevuthasan, S., Microstructure of Zro2–Ceo2 Hetero-Multi-Layer Films Grown on Ysz Substrate. *Acta Mater.* **2005,** *53*, 1921-1929.
70. Ernst, F.; Pirouz, P.; Heuer, A. H., Hrtem Study of a Cu/Al2o3interface. *Philosophical Magazine A* **1991,** *63*, 259-277.
71. Trampert, A.; Ernst, F.; Flynn, C. P.; Fischmeister, H. F.; Ru¨hle, M., High Resolution Transmission Electron Microscopy Studies of the Ag/Mgo Interface. *Acta Metallurgica et Materialia* **1992,** *40*, S227-S236.
72. Lebedev, O. I.; Tendeloo, G. V.; Amelinckx, S.; Ju, H. L.; Krishnan, K. M., High-Resolution Electron Microscopy Study of Strained Epitaxial La0.7sr0.3mno3thin Films. *Philosophical Magazine A* **2000,** *80*, 673-691.
73. Zhao, L.; Cheng, Y.; Jiang, S. P., A New, High Electrochemical Activity and Chromium Tolerant Cathode for Solid Oxide Fuel Cells. *Int. J. Hydrog. Energy* **2015,** *40*, 15622-15631.
74. Appel, C. C., Zirconia Stabilized by Y and Mn: A Microstructural Characterization. *Ionics* **1995,** *1*, 406-413.
75. Jiang, N.; Wachsman, E. D., Structural Stability and Conductivity of Phase-Stabilized Cubic Bismuth Oxides. *J. Am. Ceram. Soc.* **2004,** *82*, 3057-3064.
76. Wang, F.; Brito, M. E.; Yamaji, K.; Cho, D.-H.; Nishi, M.; Kishimoto, H.; Horita, T.; Yokokawa, H., Effect of Polarization on Sr and Zr Diffusion Behavior in Lscf/Gdc/Ysz System. *Solid State Ionics* **2014,** *262*, 454-459.
77. Wang, F.; Nishi, M.; Brito, M. E.; Kishimoto, H.; Yamaji, K.; Yokokawa, H.; Horita, T., Sr and Zr Diffusion in Lscf/10gdc/8ysz Triplets for Solid Oxide Fuel Cells (Sofcs). *J. Power Sources* **2014,** *258*, 281-289.
78. Lee, K. T.; Lidie, A. A.; Yoon, H. S.; Wachsman, E. D., Rational Design of Lower-Temperature Solid Oxide Fuel Cell Cathodes Via Nanotailoring of Co-Assembled Composite Structures. *Angew. Chem.-Int. Edit.* **2014,** *53*, 13463-13467.
79. Fan, B.; Yan, J.; Shi, W., A High Performance Solid Oxide Fuel Cells Operating at Intermediate Temperature with a Modified Interface between Cathode and Electrolyte. *J. Euro. Ceram. Soc.* **2010,** *30*, 1803-1808.

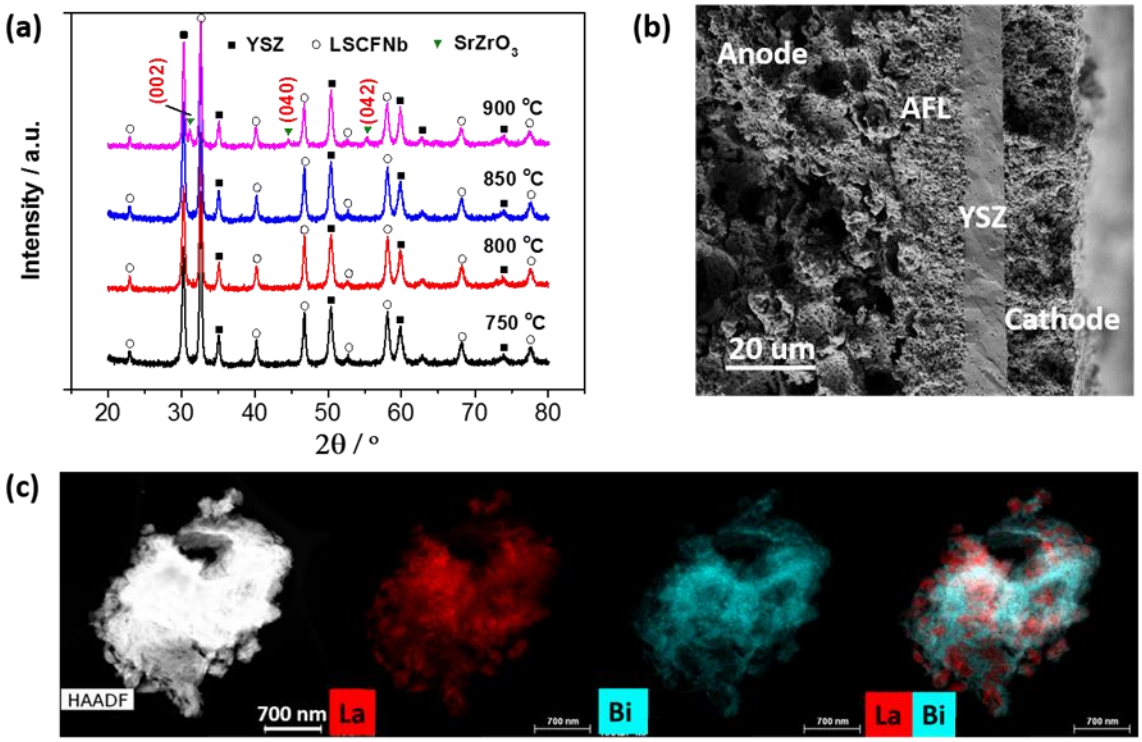

Figure 1. (a) XRD results of LSCFNb-YSZ oxide couples (1:1, w:w) sintered at 750, 800, 850, 900 °C for 2 h in air, (b) SEM image of the cross-section of an anode-supported YSZ electrolyte cell with a directly assembled ESB-LSCFNb cathode after the test. (c) STEM-EDS element mapping of as prepared ESB-LSCFNb cathode powder.

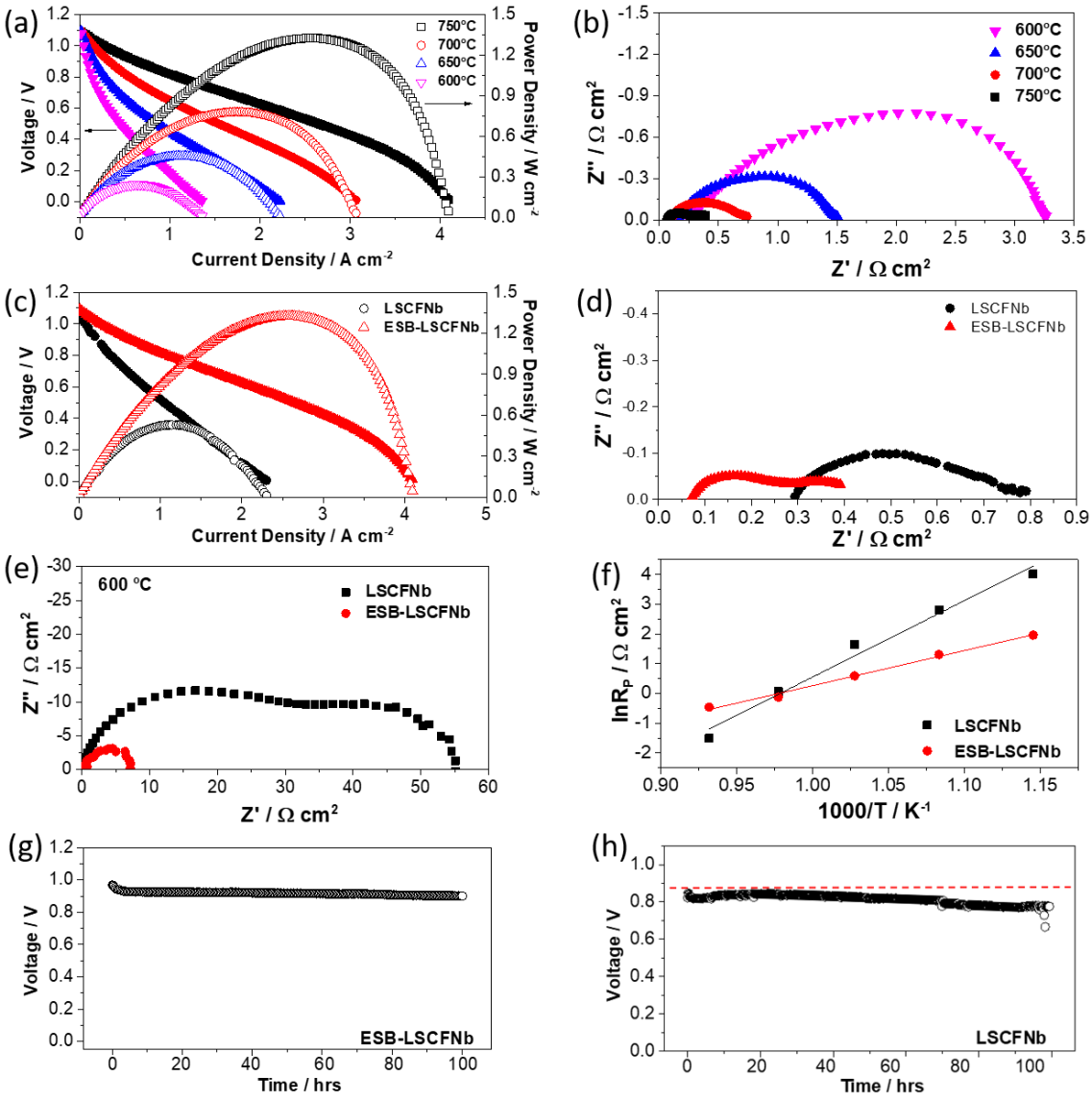

Figure 2. Electrochemical performance of anode support cell with directly assembled LSCFNb and ESB decorated LSCFNb (ESB-LSCFNb) cathodes as a function of polarization time at 750°C and 250mA cm^{-2}. (a) Polarization curves and (b) impedance spectra of the cell with ESB-LSCFNb cathode as a function of temperature. (c,d) Polarization curves and impedance curves of the cells with LSCFNb and ESB-LSCFNb cathodes at 750°C. (e) Impedance curves of the LSCFNb and ESB-LSCFNb cathodes on YSZ electrolyte supported cells measured at 600 °C. (f) Activation energy plots of R_p of LSCFNb and ESB-LSCFNb cathodes. Stability of the anode-supported cell with directly assembled (g) ESB-LSCFNb and (h) LSCFNb cathodes at 750°C and 250 mA cm^{-2}.

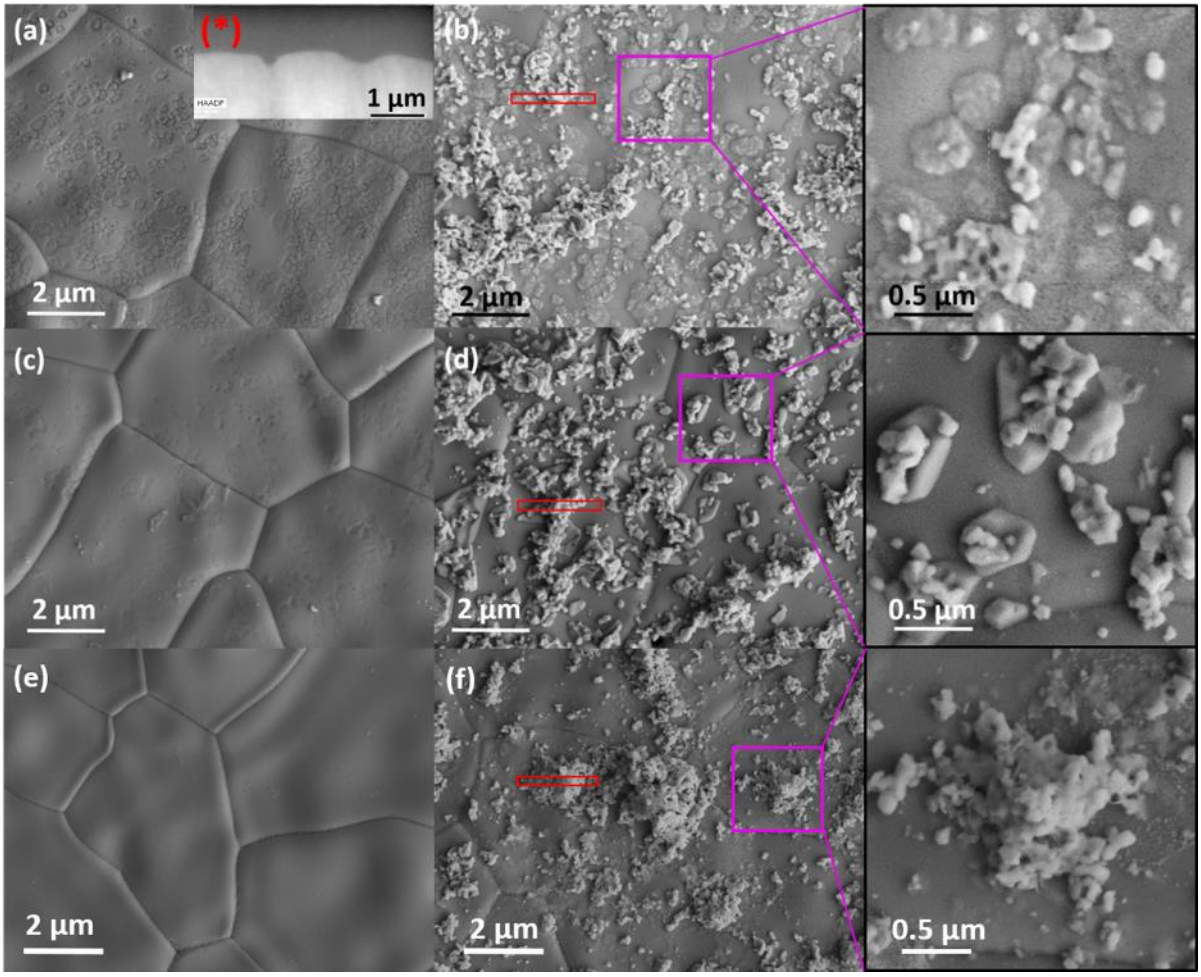

Figure 3. SEM micrographs of YSZ electrolyte surface in contact with directly assembled (a,b) LSCFNb, and (c,d) ESB decorated LSCFNb cathodes after polarization at 750°C and 250 $mAcm^{-2}$ for 100 hrs. The YSZ surface with directly assembled ESB decorated LSCFNb electrode before polarization is also shown in (e,f). The cathodes were removed by (a,c,e) acid treatment or by (b,d,f) adhesive tape. The inset (*) in (a) is the cross-section of the convex-shaped rings and red boxes in (b,d,f) indicate the locations for FIB milling.

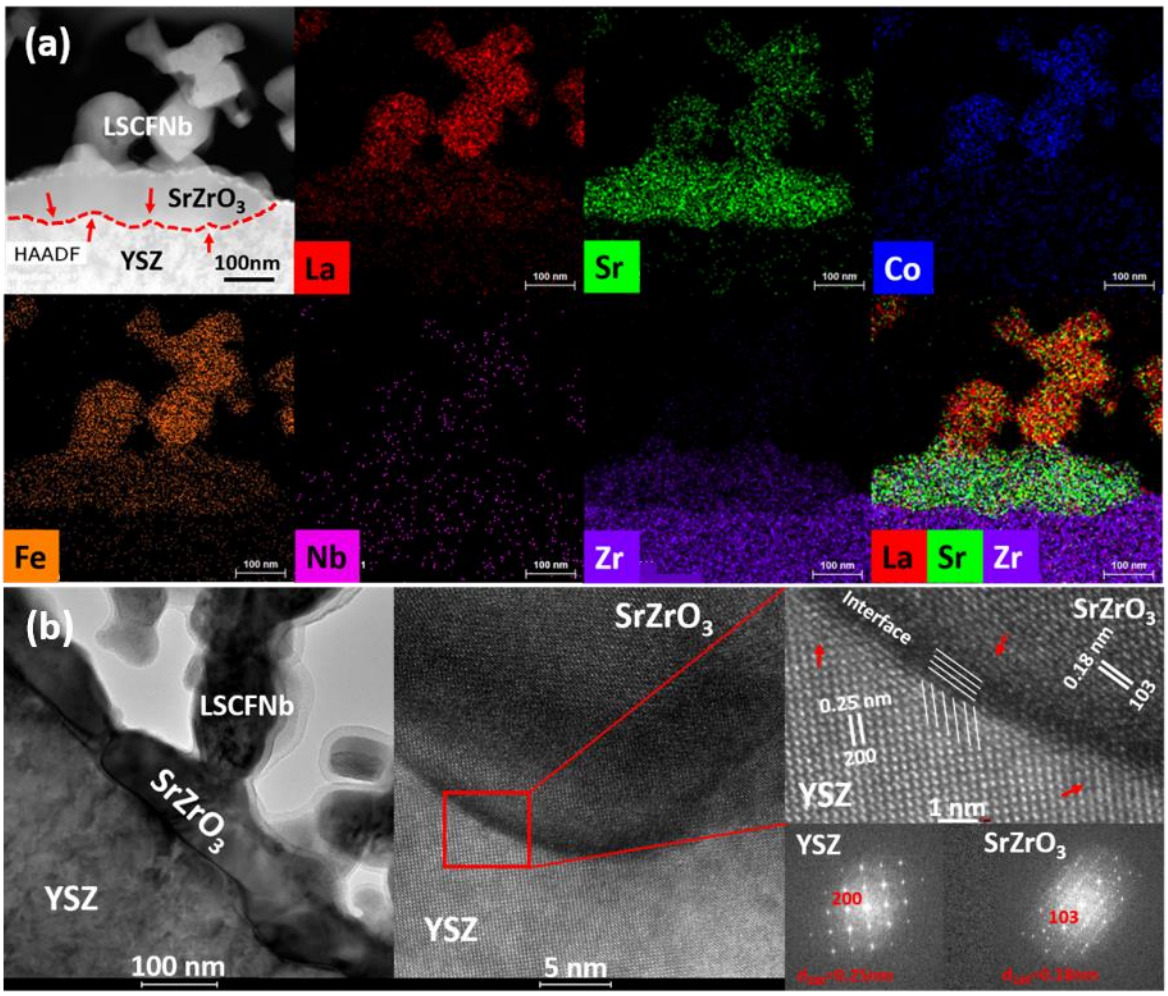

Figure 4. (a) STEM-EDS element mapping and (b) HRTEM and FFT images of the LSCFNb/YSZ interface of an anode supported YSZ electrolyte cell with a directly assembled LSCFNb electrode after polarization at 250 $mAcm^{-2}$ and 750^{o}C for 100 hrs. The red arrows in (b) indicate the lattice distortion.

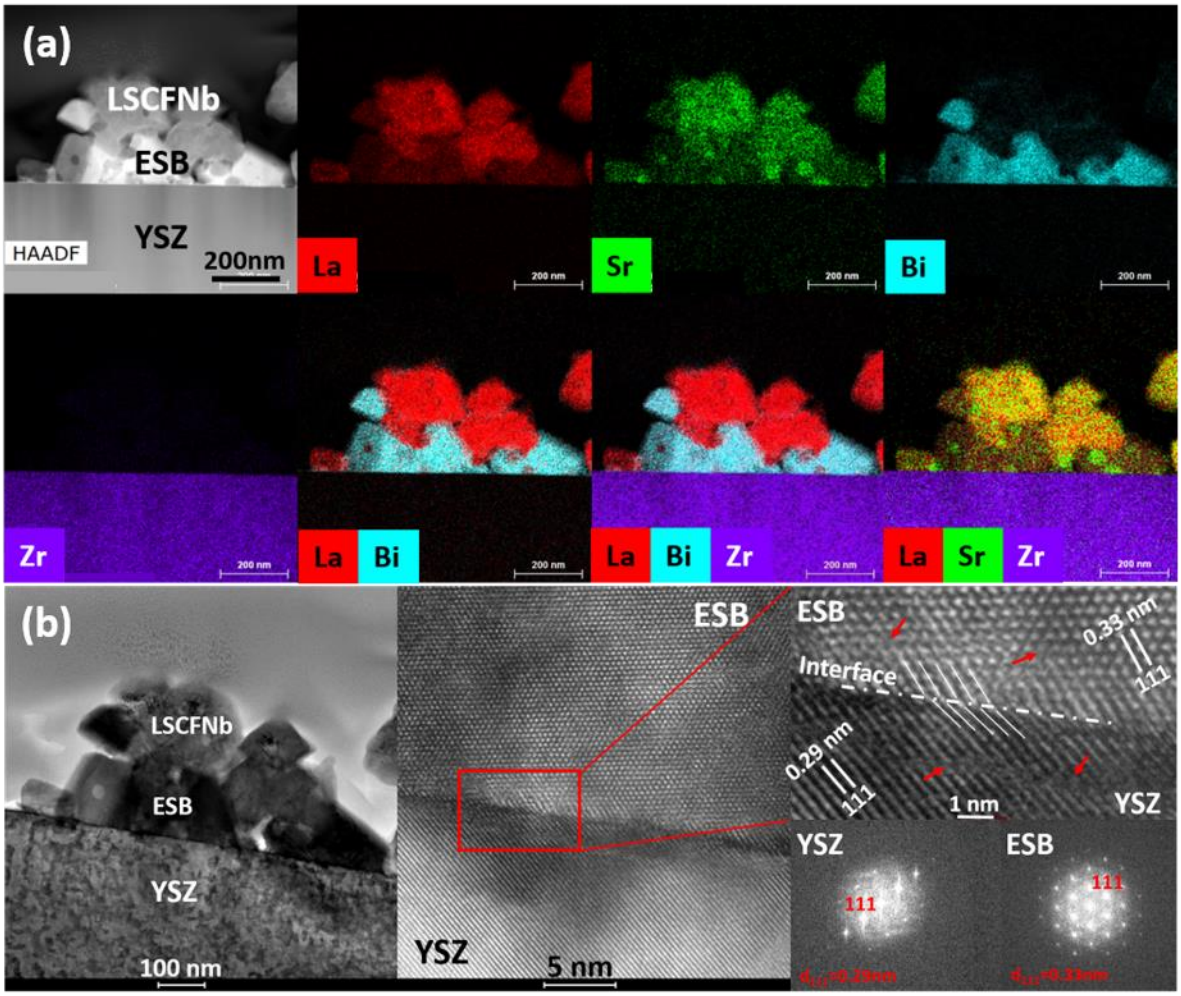

Figure 5. (a) STEM-EDS element mapping and (b) HRTEM and FFT images of the ESB-LSCFNb/YSZ interface of an anode supported YSZ electrolyte cell with a directly assembled ESB-LSCFNb electrode after polarization at 250 $mAcm^{-2}$ and 750^{o}C for 100 hrs. The red arrows indicate the lattice distortion.

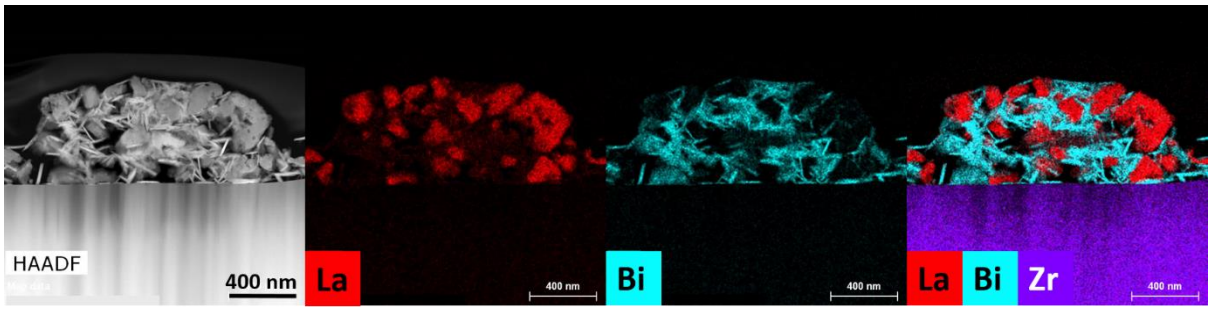

Figure 6. STEM-EDS element mapping of the ESB-LSCFNb/YSZ interface of an anode supported YSZ electrolyte cell with a directly assembled ESB-LSCFNb electrode after dwell at 750 ^{o}C for 100 hrs without polarization.

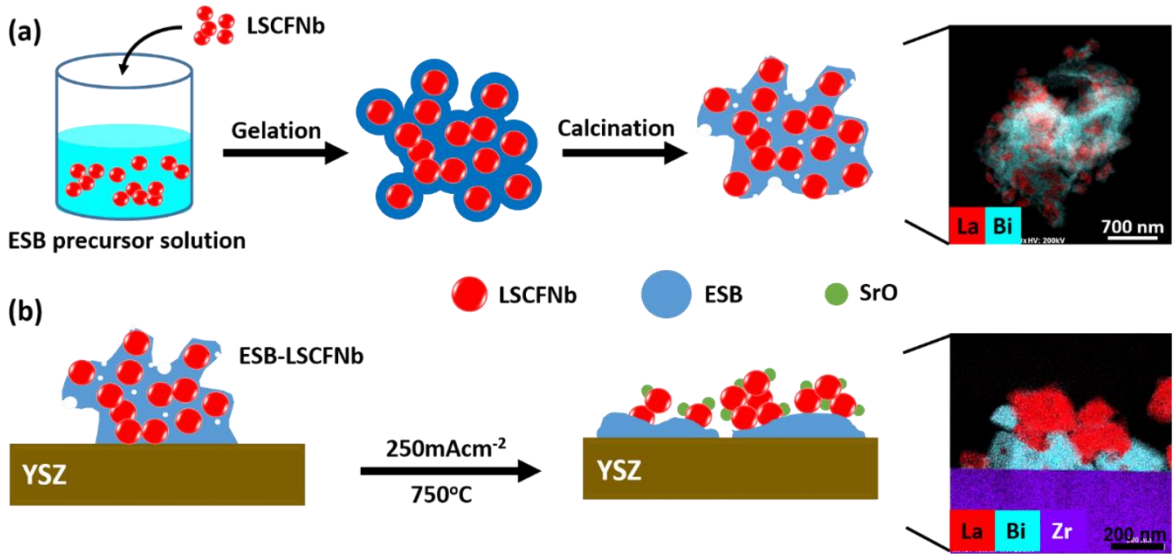

Figure 7. Schematic diagram of (a) the synthesis of ESB-LSCFNb composite cathode by decoration method and (b) the ESB-LSCFNb/YSZ interface formation under the influence of cathodic polarization at 750°C.

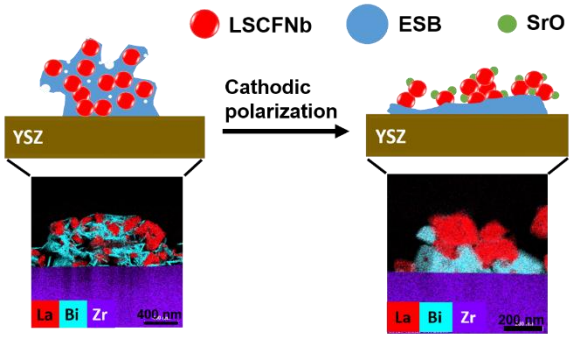

For Table of Contents Only